CONVENTIONAL/LASER DIAGNOSTICS TO ASSESS FLOW QUALITY IN A COMBUSTION-HEATED FACILITY

Ronald R. Springer* and Andrew D. Cutler†
Joint Institute for Advancement of Flight Sciences
The George Washington University
Hampton, Virginia 23681

Glenn S. Diskin‡ and Michael W. Smith§
NASA Langley Research Center
Hampton, Virginia 23681

Abstract

A study of the flow quality of the NASA Langley Direct-Connect Supersonic Combustion Test Facility (DCSCTF) is presented. The facility's nozzle exit flow field is studied through the use of a pitot rake, computational fluid dynamics (CFD), silane-seeded laser-sheet flow visualization, and coherent anti-Stokes Raman scattering (CARS). The CFD solution is shown to agree well with the pitot rake data. The flow visualization revealed the unmixedness in the facility's exit flow field. A simple modification to the design of the facility's combustion chamber is shown to yield improvement. The potential of the CARS system is demonstrated through an initial data set profiling the flow field static temperature.

Introduction

The design of supersonic combustion ramjet engines (scramjets), for air-breathing flight exceeding Mach 5, relies heavily upon the validity of computational fluid dynamic (CFD) codes in predicting supersonic mixing and chemical kinetics within the combustor. At NASA Langley's Hypersonic Airbreathing Propulsion Branch (HAPB), the CFD codes SPARK3D and VULCAN are commonly used for this purpose. In order to better understand how well these codes function, a research program has been initiated to measure temperature and species concentrations in a simplified direct-connect combustor model using the coherent anti-Stokes Raman scattering (CARS) laser diagnostic. This work is being conducted in the NASA Langley Direct-Connect Supersonic Combustion Test Facility (DCSCTF). The facility is configured to provide a Mach 2 flow with, approximately, a Mach 7 flight stagnation enthalpy, to the supersonic combustor model. This is accomplished using the facility's hydrogen/oxygen/air heater and (interchangeable) exit nozzle.

In such an experiment, the boundary conditions at the model entrance must be accurately specified. This is only possible if the facility flow is of sufficient quality, which is defined here as follows: 1) small temporal variations, and 2) a high degree of spatial uniformity. Although uniformity is not strictly required (a non-uniform boundary condition could be used in the numerical analysis), it is highly desired. With a spatially uniform flow, the experiment is less complex, and any differences between the numerical solution and experimental results can be better understood.

This paper will discuss the conventional and laser diagnostic measurements which have been undertaken in order to assess the flow quality at the nozzle exit of the DCSCTF for the proposed test program. The first of these techniques involved the design and application of a pitot rake to measure pitot pressures at the facility nozzle exit plane. A two-dimensional CFD solution for the nozzle was also performed, using VULCAN[1], for comparison with the pressure data. The second experiment was a laser flow visualization technique, which was accomplished by adding silane (SiH_4) to the facility's hydrogen supply. Silica particles (SiO_2), formed in situ, scattered light from a laser light sheet at the nozzle exit. The third technique involved the use of the CARS system to profile static temperatures at the exit plane. At this time, only limited CARS data are available.

Facility

A schematic of the DCSCTF is presented in Figure 1. This figure shows the layout of the 5 x 5 x 16 meter concrete test cell. The intake fan ventilates the entire facility with outside air. Compressed air is provided to the heater from the NASA Langley centralized air station, while hydrogen and oxygen are stored in trailers located outdoors. Within the heater, hydrogen, air, and

* Doctoral Candidate, Student Member AIAA.

† Associate Professor, Senior Member AIAA.

‡ Research Scientist, Hypersonic Airbreathing Propulsion Branch, Senior Member AIAA.

§ Research Scientist, Hypersonic Airbreathing Propulsion Branch.

Note: The inclusion of equipment brand names in this paper is for informational purposes only and should not be interpreted as an endorsement of these products by the authors, NASA, or the U.S. Government.

oxygen are burned to produce the test gas, often referred to as vitiated air. The vitiated air differs from heated air because it contains the combustion products, primarily water. This test gas is accelerated through a two-dimensional, rectangular nozzle, and then, typically, through a supersonic combustor model. Downstream of the model is a duct which can be coupled either to the atmosphere or to a 21 meter diameter vacuum sphere. The air ejector pictured in the figure was not used in this work.

A view detailing the hydrogen/oxygen/air heater is included in Figure 2. This figure shows the configuration of the toroidal manifolds and injectors which are used in the heater. Also, the ignitor, a hydrogen/oxygen torch, which is activated by an electric spark, is shown. The hydrogen injectors and ignitor depicted in the figure pass through a baffle plate and protrude slightly into the combustion chamber. The baffle plate is shown in Figure 3. It promotes mixing and uniformity of the fuel and oxidizer in the heater. Note that the ignitor is located off-center in the baffle plate. This is because the ignitor is angled so that the flame it produces will intersect the fuel exiting from the nearest hydrogen injectors. Referring again to Figure 2, note that the air and oxygen mix upstream of the baffle plate, and pass through the clearance around the hydrogen injectors and ignitor (an important point which will be addressed later) into the water-cooled combustion chamber. Finally, a two-dimensional, converging-diverging, rectangular, water-cooled, Mach 2 nozzle was used to accelerate the vitiate to the combustor model inlet conditions. The nozzle used had an exit height of 3.86 cm and width of 8.79 cm.

The facility is operated from a control room located above the facility between the intake and exhaust towers. The start-up operation of the DCSCTF is conducted as follows: 1) outside air is circulated through the test cell (for safety), 2) the air flow for the desired test point is established through the tunnel and exhausted to the atmosphere, 3) the torch ignitor is triggered on, 4) the butterfly valve is opened to direct the exhaust into the 21 meter diameter vacuum sphere (forcing the check valve closed), 5) a pilot flow of hydrogen is established through the tunnel (typically 40-50% of the desired flow rate), 6) once combustion is established, the oxygen and full hydrogen flow rate is provided to the heater, 7) shortly thereafter, the ignitor shuts off, marking the beginning of the test time. For the experiments reported herein, the run duration was typically on the order of thirty seconds.

In this work, the facility was operated at two test points. In the first case, the heater was operated, in a standard way, to produce a test gas with an oxygen mass fraction matched to that of air. This has recently been shown to be the most appropriate way to match oxygen content in a combustion-heated air simulant for the purpose of scramjet testing[2]. The second case, which is of interest from a fundamental mixing viewpoint, is an oxygen-depleted test gas. This allows mixing in a scramjet combustor model to be studied in the absence of combustion. This condition was achieved by replacing the oxygen supplied to the heater with nitrogen. The flow rates of the heater gases were set such that the total enthalpies of the two test cases were equal. Table 1 presents the test gas composition at the exit of the facility nozzle for the two cases. These values were obtained through the use of a one-dimensional, equilibrium thermodynamic analysis code. These calculations account for the heat loss to the combustion chamber cooling water, but not for heat loss in the nozzle.

Parameter	Standard Case	O_2-depleted Case
N_2 Mole Fraction	0.494	0.688
O_2 Mole Fraction	0.182	0.000
H_2O Mole Fraction	0.318	0.302
Total Temp. (K)	1946	1798
Static Temp. (K)	1284	1153
Static Press. (atm)	1.014	0.989
Mass Flow Rate (kg/s)	1.208	1.242
Mach Number	1.983	1.994

Table 1. DCSCTF test gas composition at the facility nozzle exit for the two cases investigated

Discussion of Experiment and Results

Pitot Pressure Measurements

The first set of measurements taken at the exit of the facility nozzle was a pitot rake survey. For this test, the facility was operated without any hardware connected to the downstream end of the nozzle. A catch cone, located approximately 30 cm away from the nozzle exit, was used to collect the Mach 2 test gas and couple it to the vacuum ducting. A pitot rake was installed at the nozzle exit, with the probe tips located approximately 2 mm beyond the nozzle exit plane. It should also be noted that the facility modification, to be discussed in the flow visualization section of this paper, was in place for the data presented in this section.

For this study, a new style of pitot rake was designed and successfully employed. It featured uncooled, silicon carbide probe tips attached to a water-cooled cop-

per strut, as depicted in Figure 4. The probe tip spacing is 9.5 millimeters (0.375 inches). The blue connections on top of the rake are for the cooling water. Internal passages connect the four gray probe tips to the gray connectors shown on the side of the rake. The probe tips were inserted into the copper strut and attached using a high temperature, room temperature vulcanizing (RTV), sealant/adhesive. The RTV compound was further protected with a layer of ceramic cement. The rake was an improvement over previous pitot rake hardware used in the DCSCTF which had required the use of complex, water-cooled, stainless steel probe tips[3].

The rake was mounted vertically across the nozzle's 3.86 cm height and translated horizontally across the nozzle's 8.79 cm width during each thirty second facility run. Pitot rake positioning was accomplished with a two-axis translation system in conjunction with a linear position transducer. During each run, a PC-based data acquisition system continuously recorded the four pitot pressures, facility heater pressure, and linear transducer output. Seven runs, at different vertical locations spanning the nozzle exit, allowed for 1.6 mm vertical resolution. In the horizontal direction, data was acquired approximately every 0.25 millimeters. The data consisted of 25 averaged pressure and linear position readings. For plotting, every five points were averaged together, which resulted in a horizontal grid spacing of 1.27 mm.

A great deal of care was exercised in order to minimize the error associated with the pitot pressure measurements. The five pressure transducers were calibrated against a calibration device at the same pressure that was expected during data acquisition. In addition, each of the four pitot pressure transducers were fine-tuned to read atmospheric pressure to within 69 Pa (0.01 psi) immediately before each run. In order to make certain that the four probes were in agreement with each other, one run was performed with the rake shifted vertically by 9.5 mm (equal to the probe spacing) from a previous run. This permitted the each probe's output to be compared to the others at the same location. It was discovered that three of the probes were in near perfect agreement, and one probe differed by 2%. This was accounted for in the data reduction. Based on the efforts made to reduce the measurement error, the pitot data reported herein is expected to be accurate to within 1%.

Each pitot pressure was normalized by the simultaneously recorded facility stagnation pressure. This eliminated any difference in readings that was due to variations in the heater operation between and during runs. The resulting contour plots for the standard and oxygen-depleted cases are presented in Figures 5 and 6. The plots have been drawn from the perspective of looking upstream at the nozzle exit. The theoretical value for this ratio, as determined by a one-dimensional, equilibrium thermodynamic analysis, is 0.696 for both cases. The heater pressure was approximately 7.62 atmospheres.

The results for both cases are similar, though the oxygen-depleted case has slightly higher pitot pressure ratios. The figures show that there is very little variation in the pitot pressures across the nozzle's width. Thus, the nozzle performed very two-dimensionally. The greatest lateral variation in pressure can be seen on the right-hand side of Figure 6.

A significant feature, present in both plots, are the horizontal bands of lower pressure, which are evident across the full span of the nozzle. For the standard case, these bands occur near y=1.25 and 2.5 centimeters. For the oxygen-depleted case, only the band at y=1.25 cm is present. In order to better understand these features, a computational analysis of the nozzle was performed.

Nozzle CFD Analysis

A computational fluid dynamics solution of the DCSCTF nozzle exit flow field was calculated. The problem was solved using the Viscous Upwind Algorithm for Complex Flow Analysis (VULCAN) CFD code[1]. This is one of the main CFD codes which is in use within the HAPB at NASA Langley. It is capable of handling subsonic through hypersonic, turbulent, reacting flows.

The actual nozzle wall contours were measured by the Quality Assurance and Inspection Branch at NASA Langley. The wall contours were measured near both nozzle side walls and in the center of the nozzle. These profiles were then averaged and used to represent the nozzle for the two-dimensional computational analysis. There is some asymmetry in the nozzle, as shown in Figure 7. Note that the center of the exit plane has been established as the y=0 reference in this plot, and that the wall contours are identical in the diverging section. Most of the asymmetry occurs in the subsonic portion of the nozzle where it is likely to have little effect on the exit flow. However, this region of disagreement does extend through the throat of the nozzle where it is expected to be of greater influence.

Conditions at the nozzle inlet plane were calculated based on the measured flow rates of hydrogen, oxygen (or nitrogen), and air to the facility, and on the measured combustion chamber pressure. Assuming complete reaction to equilibrium, the gas properties were determined by iterating upon the facility heat loss (to cooling water) in order to achieve the measured chamber pressure. The average flow rates and pressures, for the seven runs which comprised each pressure data set, were used as input conditions to these calculations.

The grid used in the CFD calculations consisted of

197 points distributed lengthwise and 257 points across the nozzle. It is depicted in Figure 8. In the lengthwise direction, the grid was clustered around the nozzle's throat. In the other direction, the grid was clustered near the walls. Wall functions were used for the wall boundary conditions in order to reduce the clustering requirements and improve computational efficiency. The wall clustering resulted in wall units (y^+) that ranged from seven to twelve throughout the nozzle for the grid points nearest to the walls. This choice also resulted in a subsonic Mach number at these points, which assures that reflected waves are properly treated by the wall function boundary condition.

At the nozzle inlet, the major species were specified. The calculation was performed with frozen chemistry throughout the nozzle. The full Navier-Stokes equations were solved elliptically for the entire nozzle. A two-equation turbulence model by Menter was used[4]. Low turbulence levels were assumed at the nozzle inlet (turbulent intensity = 0.01, turbulent to laminar viscosity ratio = 0.01). The water-cooled nozzle walls were assumed to be isothermal and at 500 K. Since the nozzle walls were not instrumented with thermocouples, this temperature was an estimate. However, the solution for pitot pressure changed insignificantly when the isothermal wall temperatures were varied by +/- 200 K.

The grid shown is the finest of three grids that were used. The pitot pressure solution presented here did not differ appreciably from the solution on the medium grid, which consisted of 129 x 129 points. This established the convergence of the fine grid, i.e. the solution is independent of the grid. Convergence of the solution was achieved by iterating to reduce the residual eight orders of magnitude.

The computational results for the standard case are compared with the pitot rake data in Figures 9 and 10. The results are shown using the same nozzle exit coordinates as in Figures 5 and 6. The pitot rake data shown here is an average of data over a span of five centimeters in the center of the nozzle. Figure 10, which shows the data of Figure 9 in greater detail, is shown with 1% error bars on the experimental data. The CFD solution falls within the error bars for nearly all of the data points. Most of the data was slightly lower than the CFD result. Also, note that the CFD solution is not symmetric, which is due to the nozzle wall asymmetry. The dips in pitot pressure near the center of the nozzle (noted earlier) were also present in the CFD solution. The experimental data, however, does indicate a greater drop in pressure, especially at the y= 2.5 cm location.

Similar plots for the oxygen-depleted case are presented in Figures 11 and 12. There is greater agreement for this case, as the CFD solution goes through the center of a large number of the error bars. Also note that there is essentially no difference between the CFD pitot pressure solutions for the standard and oxygen-depleted cases.

Earlier it was mentioned that a one-dimensional analysis of the nozzle yielded a theoretical pitot pressure ratio of 0.696. The CFD results predict values above this in the majority of the flow field. Due to the presence of boundary layers, the nozzle does not expand the test gas as much as the one-dimensional calculation predicts. The inclusion of the boundary layer in the CFD analysis results in lower Mach numbers and higher static pressures, which, in turn, yield higher pitot pressure ratios.

Silane-Seeded Flow Visualization

The next technique that was employed to assess flow quality was laser-sheet flow visualization. This technique was previously used in the visualization of hydrogen fuel injected into a supersonic flow[5]. It involved the injection of silane (SiH_4) into the flow (mixed with the hydrogen fuel) to produce fine (~0.25μm) seed particles. In this case, silane was injected with the hydrogen into the heater to seed the bulk flow. When the hydrogen reacts in the facility heater, the silane does as well, producing silica (SiO_2) particles in situ. The particles are sufficiently small to follow the flow, even in supersonic regions. Thus, the presence of a high concentration of particles in the flow can be correlated with high temperature.

As for the pitot rake measurements, the nozzle was configured without any attached hardware for this test. A sheet of laser light from a pulsed, frequency-doubled, Spectra-Physics GCR-4 Nd:YAG laser (532 nm) operating at 30 Hz, was used to illuminate the particles at the facility nozzle exit. The layout of the sheet-forming optics is illustrated in Figure 13. A CCD camera was used to image the Mie scattering signal and a PC-based frame grabber was used to capture 364 images during each facility run. The camera was located approximately one meter from the nozzle exit plane, and just to the right of the exit flow depicted in Figure 13. The laser firing was synchronized with the camera's shutter to insure that the 10 ns laser pulse occurred during the 100 μs camera shutter window. The laser sheet contained approximately 200 mJ of energy per pulse, but only the middle third of the sheet was distributed across the nozzle exit. This improved the uniformity of the laser sheet. A 50 mm focal length lens was used with the CCD camera, which was stopped open at f/2.0 to reduce optical speckle noise[6]. The lens was equipped with an interference filter, which passes at 532 nm, to reduce broadband luminescence from the hot particles and a 23% transmittance N.D. fil-

ter to control exposure.

The primary difficulty encountered with the visualization technique was the presence of relatively large foreign particles in the facility flow. These particles were thought to be a result of the gradual ablation of the tip of the torch ignitor over time. They were present on the left side of the flow field more often, which corresponds with the location of the ignitor tip. The particles effectively placed a lower limit on the amount of silane which needed to be added to the hydrogen. Enough silane had to be added to the flow that silica particles dominate the scattering by the unwanted particles. A few typical images of scattering by the foreign particles in the absence of silane addition are presented in Figure 14. The laser sheet and optical equipment used in this experiment would have allowed for lower percentages of silane were it not for the presence of these particles. Less silane is desirable because the large difference in density between hydrogen and silane, and the differences in heat release during combustion, could lead to a flow which differs from the unseeded flow.

With the experimental configuration described above, it was possible to achieve high quality images using only 0.13% silane, by mole, in the facility's hydrogen supply. Considering the following two reactions,

$$SiH_4 + 2\ O_2 \Longrightarrow SiO_2(s) + 2\ H_2O$$

$$H_2 + \tfrac{1}{2} O_2 \Longrightarrow H_2O$$

the heat release due to the silane reaction is 0.8% that of the hydrogen reaction, per mole of the silane/hydrogen mixture. Thus, the silane addition is believed to have an insignificant effect on the facility's performance.

Qualitative analysis of the Mie scattering images for the standard and oxygen-depleted cases revealed an alarming degree of unsteadiness and non-uniformity in the nozzle exit flow. Typical images of some of the large scale structures in the flow are presented in Figure 15. It was theorized that these structures were due to a large clearance around the ignitor, where it passed through the baffle plate, that permitted off-center oxidizer passage into the heater, away from the hydrogen injectors (see Figure 3). The structures look like low Reynolds number mixing structures (large scale), despite being present in a supersonic flow. Thus, it was theorized that these structures were generated upstream at the baffle plate mixing region, and were convected downstream.

After the observation of the flow non-uniformity, this gap around the ignitor was sealed so that all of the oxidizer had to pass through the gaps around the hydrogen injectors. The imaging was repeated and the exit flow showed a much greater degree of uniformity. Several typical images are provided in Figure 16. This result is consistent with a composition survey of the DCSCTF performed in 1974, in which it was found that "the most sensitive phenomenon which affected the profiles was the uniformity of the air distribution supplied to the combustion chamber."[3] It was in this study that the need for a baffle plate to improve spatial uniformity and enhance mixing in the heater was determined. The findings in the current work have taken this result one step further by restricting flow through the baffle plate to regions in close proximity to the hydrogen injectors, which are placed symmetrically around the periphery of the combustor.

A drawback to this modification is that higher heat loads are placed upon the tip of the ignitor. This may increase the problem of ignitor tip ablation and further contaminate the facility flow, although the flow images did not show a radical change in the concentration of contaminant particles after the fix. Reducing the number of particles is still a priority. During the operation of the CARS system, whenever a particle is present in the measurement volume, no meaningful data can be obtained. Therefore, a variety of ignitor tips have been fabricated from nickel, copper, and monel for testing as a replacement for the standard stainless steel tip. Another problem encountered involved the ignitor tip thermocouple, which is used to verify combustion. After the modification, the tip thermocouples no longer survived a single facility run. As a result, the thermocouple had to be eliminated and an alternate method of verifying ignitor operation had to be developed. An optical detection system was considered, however, the pressure rise in the combustion chamber due to ignitor operation proved to be an acceptable means of monitoring its performance.

CARS Temperature Measurements

Coherent anti-Stokes Raman scattering (CARS) is currently being applied to the nozzle exit flow. For this test, the measurements are located 12.1 cm downstream of the nozzle exit plane, inside a constant area duct that was mated to the nozzle. The side walls of the duct are equipped with vertical slits at the measurement location, which permits access by the CARS system.

The CARS diagnostic allows for the determination of the static temperature in the flow at a point. A two-axis translation system allows temperature measurement over the entire measurement plane. The CARS signal contains information on the rotational and vibrational state populations in the nitrogen molecule. This can be fit to a theoretical library, built as a function of temperature and nitrogen concentration. Sandia's CARSFT code[7] is being used to generate the libraries for this work. For further details on the CARS technique, see References 8 and 9.

Previous CARS measurements have been performed in the DCSCTF[10]. The CARS system used in this

work is an upgraded version of the one used in the previous work. The current system features a more energetic, higher pulse rate laser (30 Hz) and the added capability of measuring the concentration ratio between hydrogen and water when both are present in the measurement volume (not likely in the nozzle exit flow). Complete details of the current system will be provided at a later time when the measurements have been completed.

The current status is that the CARS system is being reconfigured in an effort to increase the signal strength. The CARS signal strength decreases as the static temperature of the measured fluid increases (roughly, with the square of the temperature). The CARS system must be capable of measurements in a supersonic combustion environment with static temperatures exceeding 2000 K. The signal strength is marginal even at the nozzle exit static temperature (near 1200 K). Based on the past success with CARS in the DCSCTF, the current problems are believed to be due to the poor spatial mode of the Nd:YAG laser at the measurement location.

Despite the low signal level, a facility run has been completed where the signal was strong enough to be fit for temperature. Unfortunately, during this run the regulator supplying hydrogen to the facility malfunctioned, resulting in flow rate oscillation. Results from this run are plotted in Figure 17 for a fixed measurement location at the center of the nozzle exit. The figure shows the CARS data superimposed on the variation in facility total temperature. This was an attempt at a standard case run. However, the facility total temperature oscillated around 1840 K, short of the desired value of 1946 K. The data in Figure 17 are plotted on two different scales to illustrate the phase relationship between the two temperatures.

CARS temperatures are measured 30 times per second. The areas in Figure 17 which lack data indicate that the signal strength was too low to be utilized. Because of the dependence of signal strength on temperature (mentioned above), it is expected that this CARS data set is biased toward low temperatures. The CARS data in the figure show evidence of being periodic with the facility total temperature. This is most evident with the two leftmost peaks. Note that coincident with the next two peaks there is a noticeable lack of CARS data. This further suggests that the high temperature data was often too low in signal strength to be detected during this run.

Conclusions

An exit flow study of the Direct-Connect Supersonic Combustion Test Facility was conducted. These measurements were performed to determine what degree of unsteadiness and spatial uniformity exists in the flow. Pitot pressure measurements were performed using a newly designed pitot rake. A computational fluid dynamics solution was obtained, using VULCAN, for comparison with the pitot rake results. Laser-sheet flow visualization was conducted in order to assess temperature variations within the test gas. Currently, a coherent anti-Stokes Raman scattering diagnostic is being used to quantitatively address the temperature variations.

The experimentally measured pitot pressures show little variation across the nozzle's width. However, in the vertical direction there is some variation. The pitot pressure is relatively constant over a 2.3 cm region in the center of the nozzle's 3.86 cm height. The regions within 1.3 and 7.5 millimeters of the top and bottom walls show a gradual decay in pitot pressure as the wall is approached. Within 1.3 mm of the top and bottom wall, the drop in pitot pressure is very rapid. This is representative of the nozzle's boundary layer. The VULCAN solution shows excellent agreement with these experimental observations.

Redesign of the nozzle wall contours could be done to yield flat pitot pressure profiles (outside of the boundary layer). However, this is cost-prohibitive. In addition, the facility is operated over a wide range of flight enthalpies between Mach 4 and 7.5. No single nozzle can work perfectly over this wide range of conditions with varying test gas properties.

Another important observation is that the pitot pressures showed no significant change before (data not included) and after the facility was modified to reduce temperature fluctuations. Thus, the pitot pressure may be insensitive to variations in some of the more important parameters which are important in a combustion experiment. This has been seen before. In Reference 3, it was noted that the pitot pressure showed no change when the flow field possessed 600 K variations in total temperature, compared to a case with uniform total temperature.

One may wish to use the complete VULCAN solution as input conditions to the numerical analysis of a combustor model installed in the facility. The pitot rake data does serve to validate the results of the CFD. However, based on the arguments of the preceding paragraph, this should not be done yet. A quantitative experiment must be conducted to assess temperature variations, in support of the qualitative flow visualization results. This is the objective of the current work with coherent anti-Stokes Raman scattering.

References

[1]White, J. A. and Morrison, J. H., "A Pseudo-Temporal Multi-Grid Relaxation Scheme for Solving the Parabolized Navier-Stokes Equations," AIAA Paper 99-3360, June 1999.

[2]Cutler, A. D., "Specification of Model Entrance Conditions for Scramjet Testing in Vitiated Air," *AIAA Journal*, **36**(7), 1200-1207 (1998).

[3]Eggers, J. M., "Composition Surveys of Test Gas Produced by a Hydrogen-Oxygen-Air Burner," NASA TM X-71964, June 1974.

[4]Menter, F. R., "Improved Two-Equation k-ω Turbulence Model for Aerodynamic Flows," NASA TM-103975, 1992.

[5]Smith, M. W. and Northam, G. B., "Instantaneous Planar Visualization of Reacting Supersonic Flows Using Silane Seeding," AIAA Paper 91-1690, June 1991.

[6]Smith, M. W., "The Reduction of Laser Speckle Noise in Planar Doppler Velocimetry Systems," AIAA Paper 98-2607, June 1998.

[7]Palmer, R. E., "The CARSFT Computer Code for Calculating Coherent Anti-Stokes Raman Spectra: User and Programmer Information," Sandia Report SAND89-8206

[8]Eckbreth, A. C., *Laser Diagnostics for Combustion Temperature and Species*, Abacus Press, 1988.

[9]Druet, S. and Taran, J. P., "CARS Spectroscopy," *Progress in Quantum Electronics*, **7**, 1-72 (1981).

[10]Smith, M. W., Jarrett, O. Jr., Antcliff, R. R., Northam, G. B., Cutler, A. D., and Taylor, D. J., "Coherent Anti-Stokes Raman Spectroscopy Temperature Measurements in a Hydrogen-Fueled Supersonic Combustor," *Journal of Propulsion and Power*, **9**(2), 163-168 (1993).

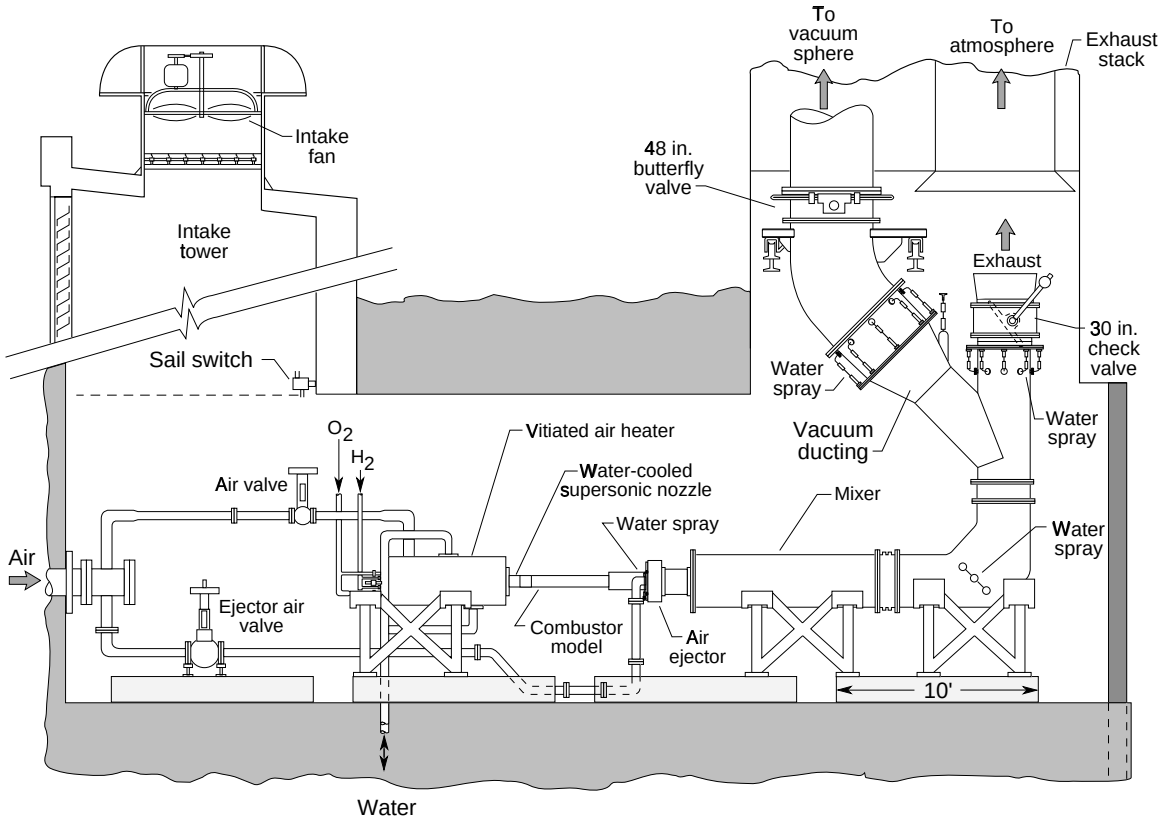

Figure 1. An illustration of the Direct-Connect Supersonic Combustion Test Facility (DCSCTF)

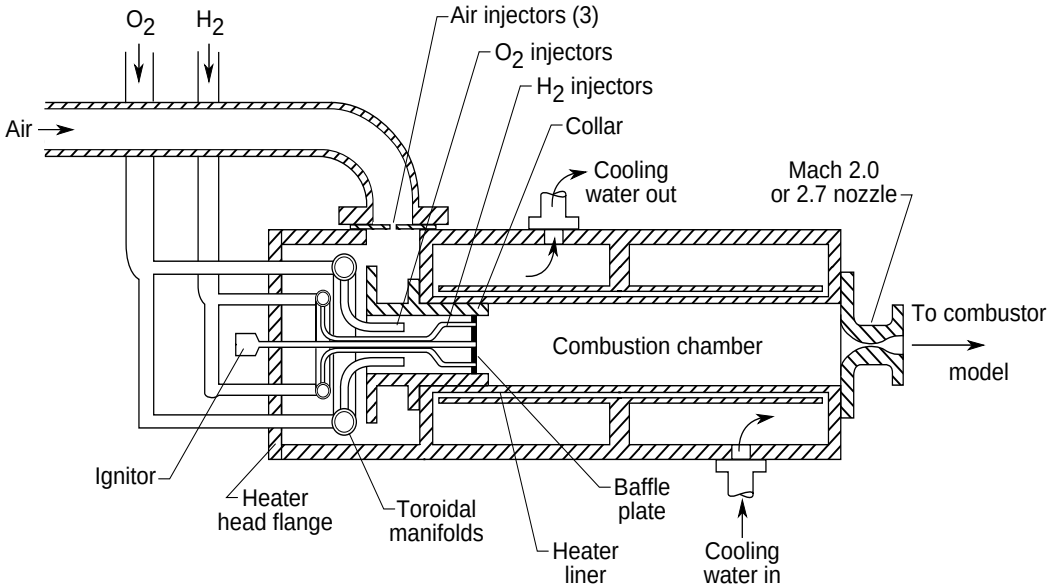

Figure 2. A cut-away view of the vitiated air heater for the DCSCTF

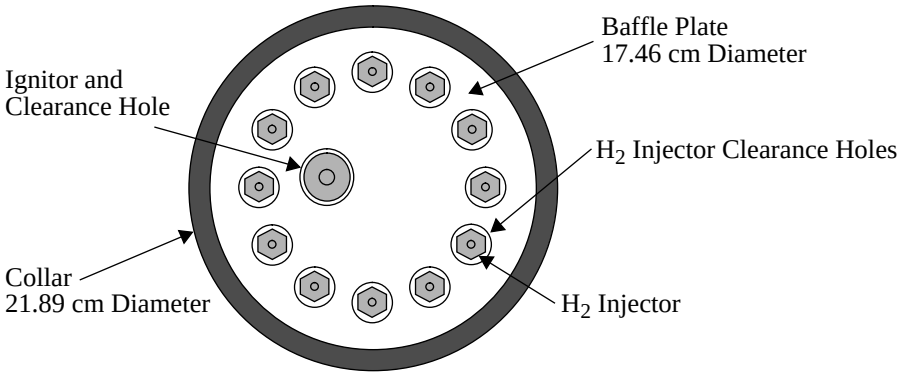

Figure 3. View of the baffle plate
(looking upstream from within the combustion chamber of the DCSCTF)

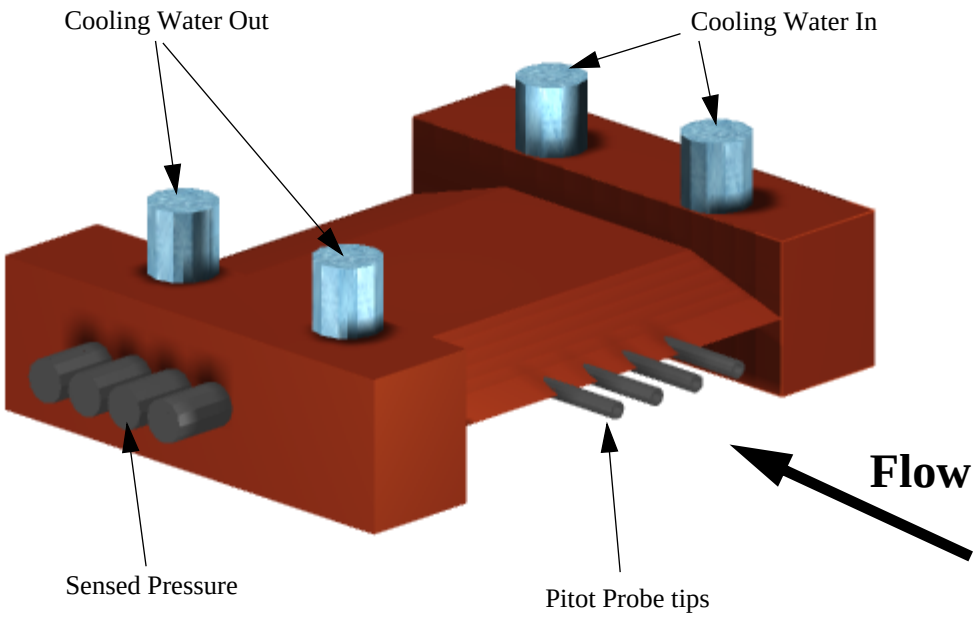

Figure 4. Copper, water-cooled pitot rake with silicon carbide probe tips

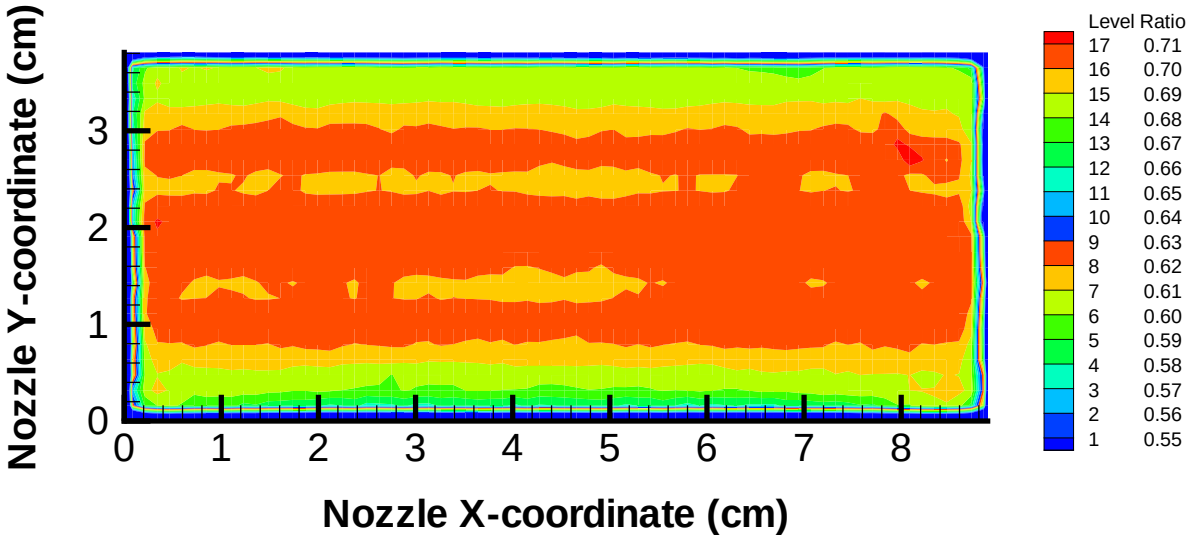

Figure 5. Ratio of pitot pressure to heater combustion chamber pressure for the standard case

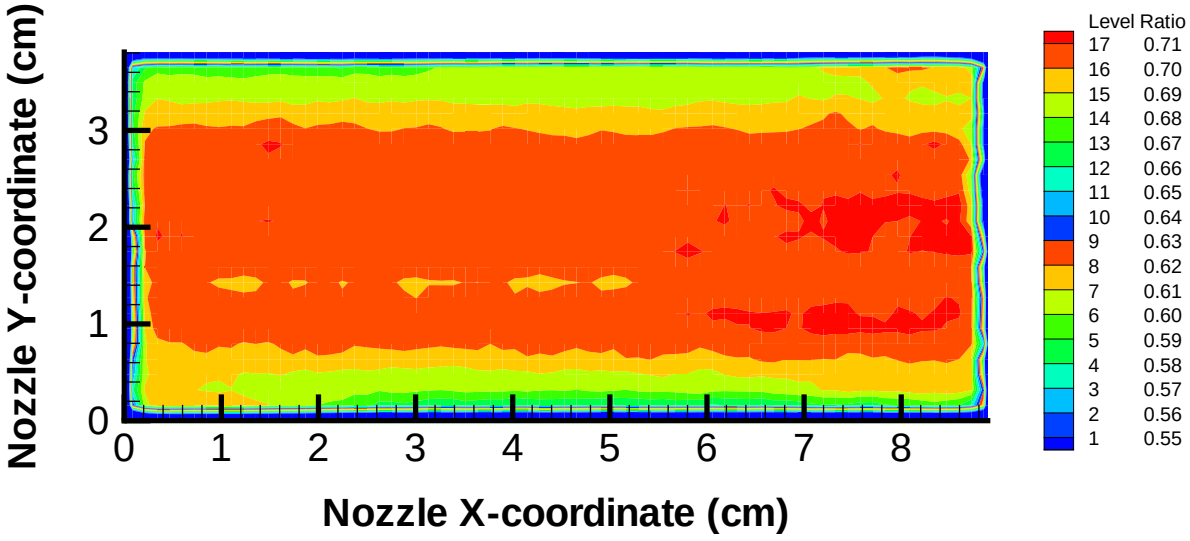

Figure 6. Ratio of pitot pressure to heater combustion chamber pressure for the oxygen-depleted case

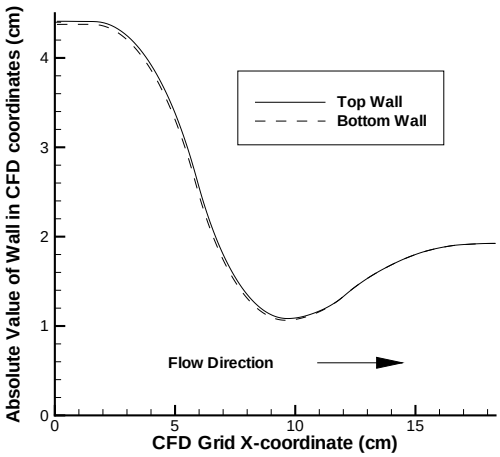

Figure 7. Average nozzle wall contours shown in the CFD grid coordinate system

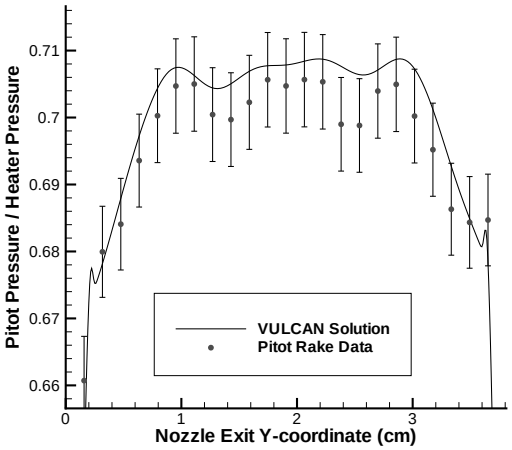

Figure 10. Detailed view of the data from Figure 9 with 1% error bars shown

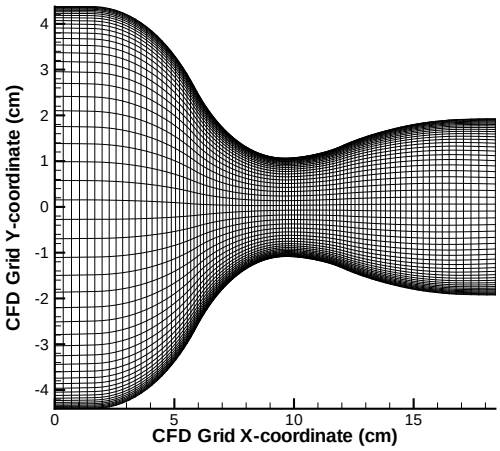

Figure 8. VULCAN computational grid (every other point shown in x-dir., every five in y-dir.)

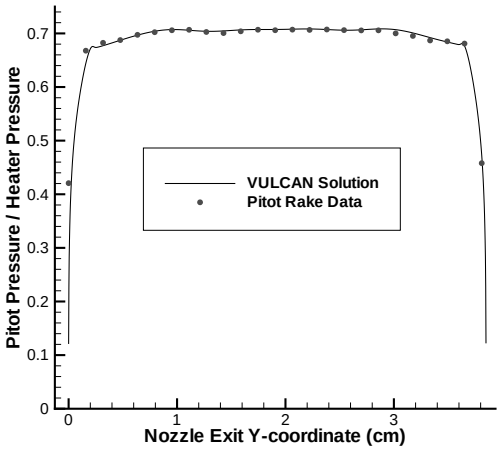

Figure 11. Comparison of pitot rake data and VULCAN solution for the oxygen-depleted case

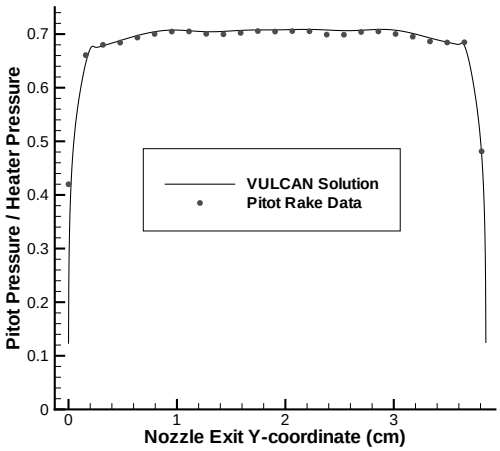

Figure 9. Comparison of pitot rake data and VULCAN solution for the standard case

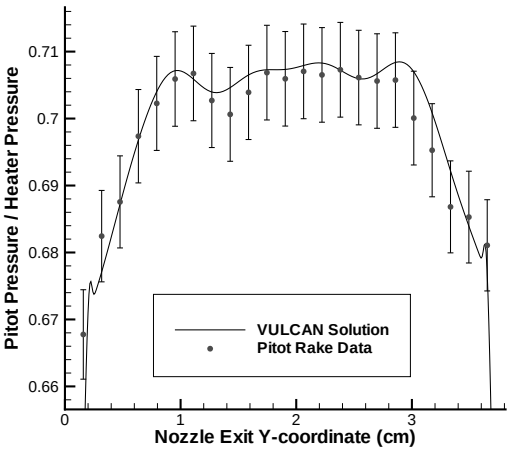

Figure 12. Detailed view of the data from Figure 11 with 1% error bars shown

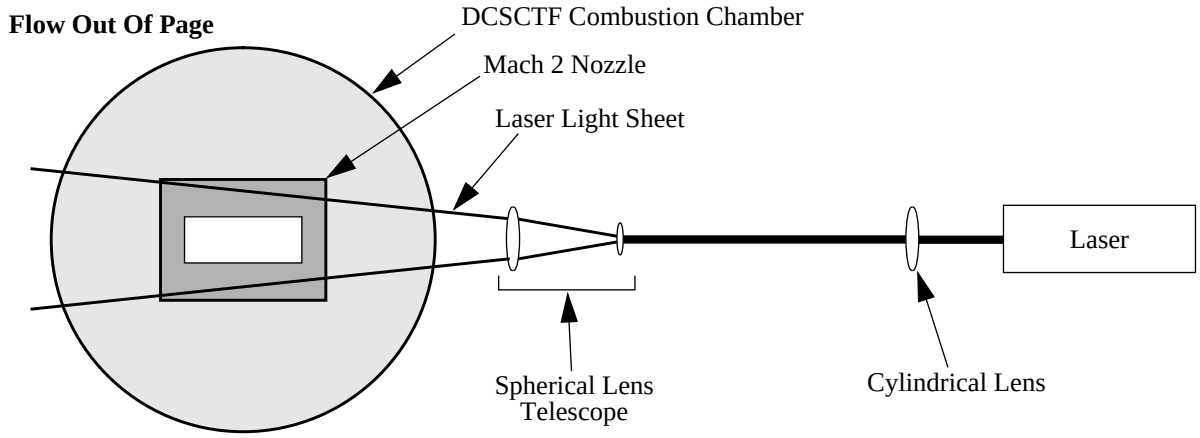

Figure 13. Diagram of the optical configuration for the laser-sheet flow visualization experiment

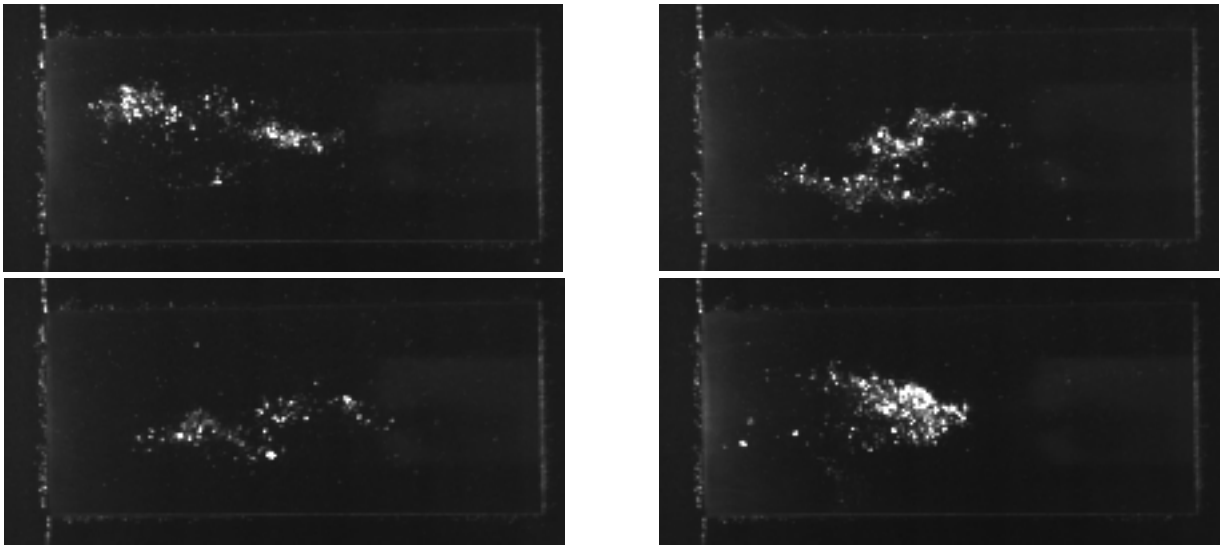

Figure 14. Nozzle exit visualization of heater particles (raw images)

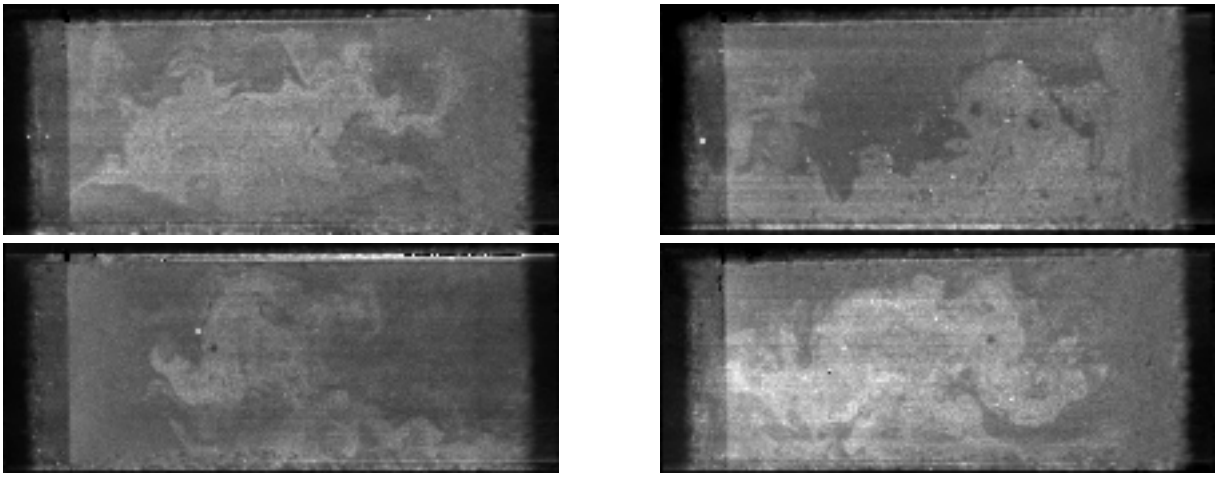

Figure 15. Mie scattering images illustrating unsteady, non-uniform flow
(images processed to remove laser sheet non-uniformity)

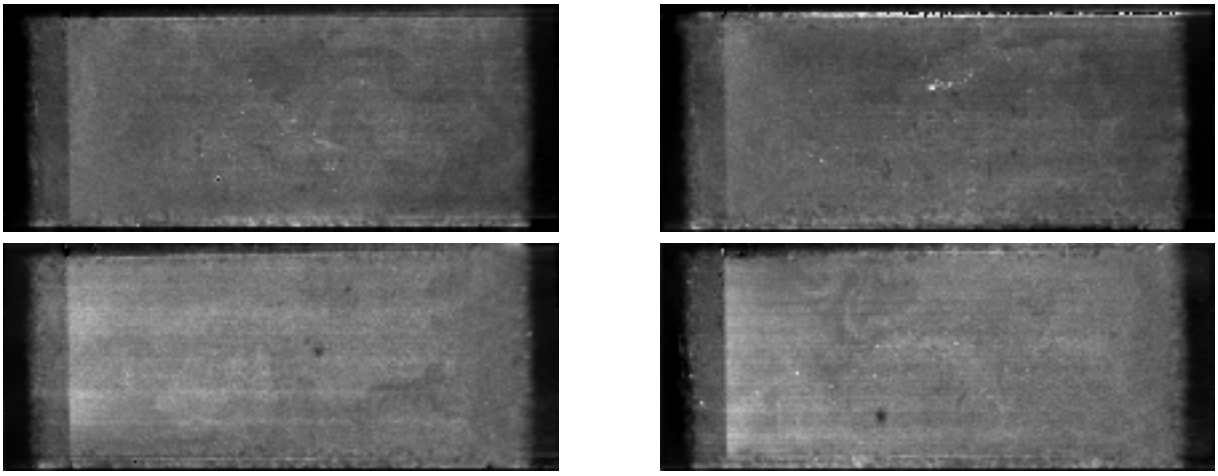

Figure 16. Mie scattering images typical of those acquired after the facility modification (images processed to remove laser sheet non-uniformity)

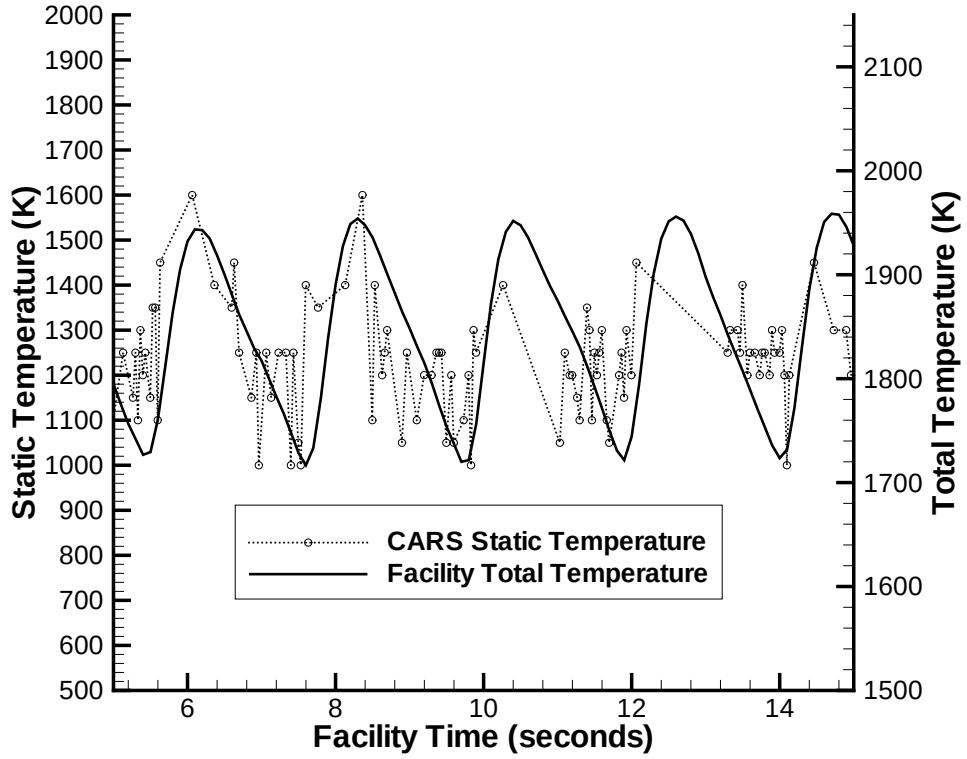

Figure 17. Comparison of CARS static temperature with oscillation in DCSCTF calculated total temperature (CARS measurement was conducted in the center of the nozzle and 12.1 cm downstream)